Neutron one-quasiparticle states in $^{251}Fm_{151}$ populated via the α decay of ^{255}No

M. Asai,[1] K. Tsukada,[1] H. Haba,[2] Y. Ishii,[1] T. Ichikawa,[3] A. Toyoshima,[1] T. Ishii,[1] Y. Nagame,[1] I. Nishinaka,[1] Y. Kojima,[4] and K. Sueki[5]

[1]*Advanced Science Research Center, Japan Atomic Energy Agency, Tokai, Ibaraki 319-1195, Japan*
[2]*Nishina Center for Accelerator-Based Science, RIKEN, Wako, Saitama 351-0198, Japan*
[3]*Yukawa Institute for Theoretical Physics, Kyoto University, Kyoto 606-8502, Japan*
[4]*Graduate School of Engineering, Hiroshima University, Higashi-Hiroshima 739-8527, Japan*
[5]*Department of Chemistry, University of Tsukuba, Tsukuba, Ibaraki 305-8571, Japan*

(Received 7 November 2010; published 27 January 2011)

Excited states in ^{251}Fm populated via the α decay of ^{255}No are studied in detail through α-γ coincidence and α fine-structure measurements. Five excited states reported previously in ^{251}Fm are firmly established through the α-γ coincidence measurement, and rotational bands built on one-quasiparticle states are newly established through the α fine-structure measurement. Spin-parities and neutron configurations of the excited states in ^{251}Fm as well as the ground state of ^{255}No are definitely identified on the basis of deduced internal conversion coefficients, lifetimes of γ transitions, rotational-band energies built on one-quasiparticle states, and hindrance factors of α transitions. It is found that the excitation energy of the $1/2^+[620]$ state in $N = 151$ isotones increases with the atomic number, especially at $Z \geqslant 100$, while that of the $1/2^+[631]$ state decreases at $Z = 100$. Ground-state deformations and energies of neutron one-quasiparticle states in the $N = 151$ isotones are calculated using a macroscopic-microscopic model, and the energy systematics of the one-quasiparticle states in the isotones are discussed in terms of the evolution of nuclear deformation involving the hexadecapole (β_4) and hexacontatetrapole (β_6) deformations.

DOI: 10.1103/PhysRevC.83.014315 PACS number(s): 21.10.Hw, 23.20.Lv, 23.60.+e, 27.90.+b

I. INTRODUCTION

Nuclei located in the region of proton number $Z > 100$ and neutron number $N > 150$ exhibit a variety of intriguing nuclear structure aspects. The existence of large deformed shell gaps at $N = 152$ and 162 is one of the interests. These shell gaps are clearly seen in the systematics of experimental Q_α values [1] which exhibit an irregular increase from $N = 152$ to 154 (or $N = 162$ to 164), indicating that the nuclei at $N = 152$ (162) are more bound than those at $N = 154$ (164). Both gaps are called "deformed shell gaps." However, theoretical calculations by the macroscopic-microscopic models revealed a considerable difference between them [2]. The $N = 152$ gap is mainly generated by large quadrupole deformation with a deformation parameter $\beta_2 \sim 0.25$, while the $N = 162$ gap is generated by a significant contribution of large negative hexadecapole deformation β_4. In addition, theoretical calculations predict the appearance of large negative hexacontatetrapole deformation β_6 around $^{252}Fm_{152}$, which gives an additional increase of the $N = 152$ gap energy. The deformation parameters largely influence energy spacings and order of Nilsson single-particle orbitals. Experimental assignments of one-quasiparticle states in odd-mass $Z > 100$ and $N > 150$ nuclei thus give us a good opportunity to investigate the properties of the deformed shell gaps and the evolution of nuclear deformation involving the higher-order deformations of β_4 and β_6.

In this paper, we focus on the properties of the $N = 152$ deformed shell gap. This is the gap between the neutron $9/2^-[734]$ and $1/2^+[620]$ orbitals [2]. The ground-state configuration of odd-mass $N = 151$ and $N = 153$ isotones is expected to be $9/2^-[734]$ and $1/2^+[620]$, respectively, and the $1/2^+[620]$ one-quasiparticle state in the $N = 151$ isotones is expected to lie at high excitation energy owing to the large energy gap between the $9/2^-[734]$ and $1/2^+[620]$ orbitals. This indicates that the excitation energy of the $1/2^+[620]$ state in the $N = 151$ isotones becomes a good measure of the $N = 152$ deformed shell gap. The α decay of odd-mass $N = 153$ isotones is suitable to establish the $1/2^+[620]$ state in the $N = 151$ isotones, because this state is populated by a favored α transition from the $1/2^+[620]$ ground state in the $N = 153$ isotones. Moreover, the α decay of odd-mass $N = 153$ isotones populates many other one-quasiparticle states in the $N = 151$ isotones because there is a large phase space below the higher-lying $1/2^+[620]$ state.

Excited states in $^{245}Pu_{151}$, $^{247}Cm_{151}$, and $^{249}Cf_{151}$ have been studied in detail through transfer reactions, in-beam γ-ray spectroscopy, and α-, β^--, and electron capture (EC)-decay spectroscopy [3–8]. The $1/2^+[620]$ states as well as other one-quasiparticle states have been established in these nuclei. For $^{251}Fm_{151}$, there are a few experimental data on the α decay of $^{255}No_{153}$. Eskola *et al.* [9] reported five α groups in the α decay of ^{255}No, and found that their energies and intensities are similar to those of the α decay of ^{253}Fm. On the basis of this similarity, they suggested that the ground-state configuration of ^{255}No would be the same as that of the isotones, namely $1/2^+[620]$, and the 190- and 550-keV levels in ^{251}Fm would have the $5/2^+[622]$ and $1/2^+[620]$ configurations, respectively. Dittner *et al.* [10] performed an α-x/γ coincidence experiment and found that the 191-keV level has a half-life of 15.2 μs, which confirms the $5/2^+[622]$ assignment to the 191-keV level. They also reported more detailed α fine-structure data than those of Ref. [9], although

their energies and intensities deviate from the present ones. The recent α-γ decay study using a velocity filter SHIP (Separator for heavy-ion reaction products) at GSI by Heßberger *et al.* [11] firmly established the excited-state energies in ^{251}Fm through the γ-ray measurement, and their spin-parities were assigned tentatively on the basis of the deduced multipolarities of the γ transitions and the $1/2^+[620]$ assumption for the ground state of ^{255}No according to Ref. [9]. Heßberger *et al.* [11] also reported α energies and intensities of ^{255}No, although they noted that those values were not accurate because the energy sum between the α particle and the subsequently emitted conversion electrons, Auger electrons, and low-energy x rays detected simultaneously with a Si detector significantly distorted the α fine-structure spectrum. The influence of this coincidence summing effect becomes serious under the conditions such that α-decaying nuclei are implanted into a Si detector with recoil separators [11], or the α source is measured at a close source-to-detector distance as in Refs. [9,10].

In the present work, more detailed experimental studies are carried out for the α decay of ^{255}No: the α-γ coincidence measurement and the α fine-structure measurement. In particular, the α fine-structure measurement enables us to observe weak α transitions to rotational-band members built on one-quasiparticle states and to determine α energies and intensities very precisely without an influence of the coincidence summing effect. The deduced hindrance factors of the α transitions and rotational-band energies built on one-quasiparticle states are very helpful to assign the neutron configurations to the excited states. On the basis of these experimental data, we re-assign spin-parities and neutron configurations of the excited states in ^{251}Fm as well as the ground state of ^{255}No without the $1/2^+[620]$ assumption for the ground state of ^{255}No.

II. EXPERIMENT

The nucleus ^{255}No was produced in the ^{248}Cm(^{12}C,5n) reaction using the 20-MV tandem accelerator at Japan Atomic Energy Agency (JAEA). The beam energy was 77 MeV on target, and the beam intensity was 270-particle nA on average. The isotopic composition of the Cm target was 96.7% ^{248}Cm, 0.04% ^{247}Cm, 3.1% ^{246}Cm, 0.15% ^{245}Cm, and 0.008% ^{244}Cm, and the thickness of ^{248}Cm was 530 μg/cm^2, electrodeposited on a 1.8 mg/cm^2 thick beryllium backing. Reaction products recoiling out of the target were thermalized in He gas, attached onto KCl aerosol clusters in the He gas, and transported through a 25-m-long capillary with a He jet to a rotating-wheel α(-γ) detection system, where the products attached on the clusters were deposited on a 120 μg/cm^2 thick polyethylene terephthalate foil 40 (or 80 for the α fine-structure measurement) of which were set on the periphery of a rotating wheel at 9° (or 4.5°) intervals [12].

In the α-γ coincidence measurement, the wheel periodically rotated by 63° at 180 s intervals, and moved the deposited sources to two consecutive detector stations each of which was equipped with two Si PIN (*p-intrinsic-n* structure) photodiode detectors (Hamamatsu S5377-04, 28 × 28 mm^2 active area) and two Ge detectors (ORTEC LOAX and GMX). At the detector station, the source was sandwiched between the two Si detectors to detect α particles with an 87% efficiency, and the two Ge detectors were placed just behind the two Si detectors. The efficiency of each Ge detector was ∼15% for 60–120-keV γ rays; the efficiency calibration curves were measured using a mixed γ-ray standard source containing ^{241}Am, ^{109}Cd, ^{57}Co, ^{139}Ce, ^{203}Hg, ^{113}Sn, ^{85}Sr, ^{137}Cs, ^{88}Y, and ^{60}Co. The energy calibration of the Ge detectors was carried out using the same source before and after the on-line experiment. The α energy calibration was done using the α lines of ^{150}Dy, ^{153}Er, ^{244,246}Cm, ^{213}Ra, and ^{250,252,254}Fm observed simultaneously with ^{255}No in the measured α-energy spectrum. These nuclei were produced in the reactions with some impurities in the target, fusion- or multinucleon-transfer reaction products, and elastically scattered target nuclei. α singles and α-γ coincidence events were recorded in an event-by-event mode together with time information.

For the α fine-structure measurement, another rotating wheel system consisting of an 80-position rotating wheel and six Si PIN photodiode detectors (Hamamatsu S3204-09, 18 × 18 mm^2 active area) was employed. The wheel rotated by 4.5° at 90 s intervals to move the sources to six consecutive detector stations. The detectors at the first four stations were set at 12.2 mm from the deposited sources, while those of the last two were at 2.2 mm. Apertures with a 17-mm inner diameter were placed in front of the first four detectors to reduce the edge effect. Solid angles of the detectors were 10% of 4π for the first four and 39% for the last two detectors. The former setup significantly reduces the low-energy tail of α peaks as compared with the latter one, and also reduces the coincidence summing effect, which allows us to determine α energies and intensities precisely. The last two detectors were only used to obtain "distorted" α spectra to see the influence of the coincidence summing effect. The energy calibration of the Si detectors was carried out using the α lines of ^{150,151}Dy, ^{246}Cm, ^{213}Ra, ^{213}Fr, and ^{250,252,254}Fm [3] observed simultaneously with ^{255}No. Data were recorded event by event together with time information.

III. EXPERIMENTAL RESULTS

A. α-γ coincidence measurement

Figures 1(a) and 1(b) show γ-ray spectra in coincidence with 7490–8360-keV α particles which correspond to the α energy range of ^{255}No. The time window was set at the range of −100 ns to +500 ns from the prompt peak for the prompt coincidence spectrum [Fig. 1(a)], and at 0.5–47.5 μs for the delayed one [Fig. 1(b)]. Many γ lines were observed in the prompt spectrum, while in the delayed spectrum only a γ line at 200.09 keV was observed in addition to the intense Fm K and L x rays. Figures 2(a) and 2(b) show correlations between α and γ-ray energies for the prompt and the delayed coincidence events, respectively. The α singles spectrum measured in the α-γ coincidence experiment is also shown in the same figures by a histogram. The most intense α line of 8100 keV was not coincident with any prompt γ rays, but was coincident with delayed γ and x rays. This indicates that the level populated by the 8100-keV α transition should

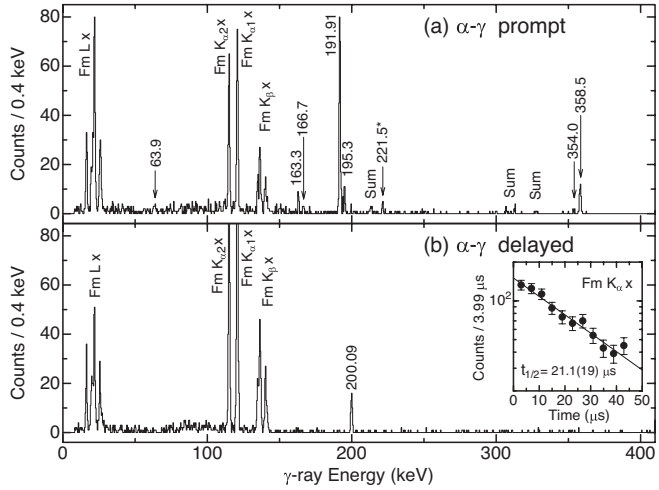

FIG. 1. Gamma-ray spectra in coincidence with 7490–8360-keV α particles, which corresponds to the α energy range of ^{255}No. (a) Prompt coincidence spectrum for which the time window was set at the range of -100 ns to $+500$ ns from the prompt peak. The 221.5-keV γ ray is attributed to the α decay of ^{253}No. (b) Delayed one of 0.5–47.5 μs. The inset shows a decay curve of Fm K_α x rays observed in the delayed coincidence spectrum.

have a long lifetime. On the basis of the measured α and γ-ray energies and the α-γ coincidence relationships, we have established the γ decay scheme in ^{251}Fm as shown in Fig. 3. Energies and relative intensities of the γ rays are summarized in Table I. Corrections for the coincidence summing effect between cascade γ transitions were carried out to deduce the γ-ray intensities.

The 200.09-keV level was found to be the isomeric state with a half-life of 21.1(19) μs which is in good agreement with the literature value of 21(3) μs [11]. The present half-life value was derived from the decay curve of Fm K_α x rays shown in the inset of Fig. 1(b). The 200.09-keV γ ray also showed the same half-life within experimental uncertainties. The half-lives of the γ rays derived from the α-γ time spectra are given in Table I. The 195.3- and 358.5-keV γ rays showed prompt time distributions; only the upper limits of $<$16 ns and

TABLE I. Energies and relative intensities of γ rays in the α decay of ^{255}No. Half-lives of the γ rays derived from the α-γ time spectra are also given.

Energy (keV)	Relative intensity[a]	Half-life
63.9(8)	1.4(9)	
163.3(2)	8.4(22)	
166.7(2)	3.9(15)	
191.91(16)	100(12)	22(3) ns
195.3(2)	12.9(30)	$<$16 ns
200.09(11)	31(5)	16(5) μs[b]
354.0(7)	4.0(18)	
358.5(2)	24(5)	$<$8 ns

[a]For I_γ per 100 α decays, multiply by 0.10.
[b]More accurate value of 21.1(19) μs was obtained from the decay curve of the Fm K_α x rays.

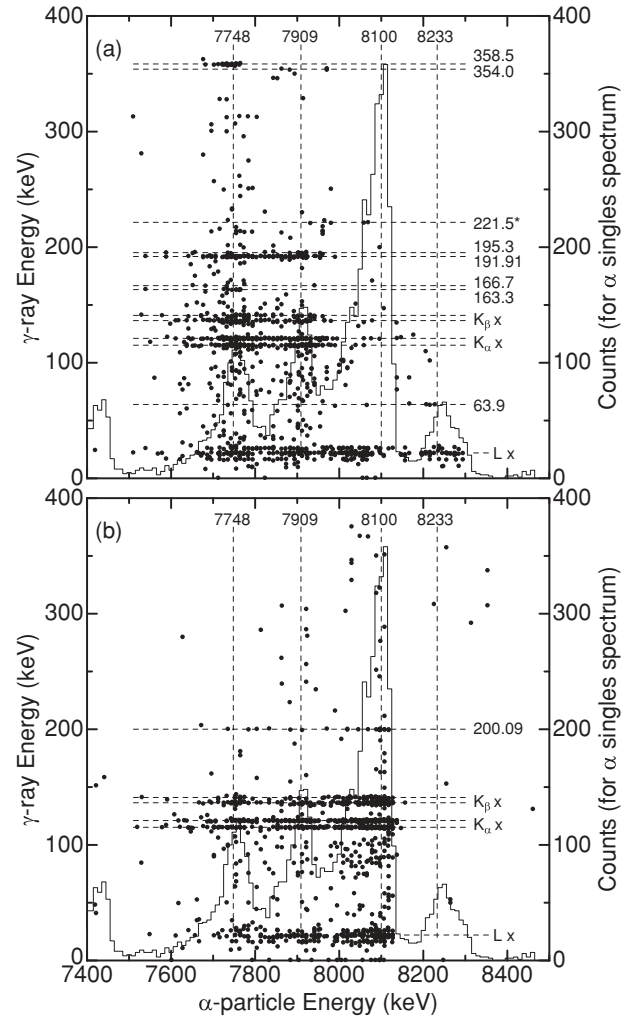

FIG. 2. Two-dimensional plots of α-γ coincidence events: (a) prompt coincidence events detected within the time interval of -100 ns to $+500$ ns, and (b) delayed ones of 0.5–47.5 μs. A histogram shows an α-singles spectrum observed in the α-γ experiment. The 221.5-keV γ-ray events are attributed to the α decay of ^{253}No.

$<$8 ns were obtained for these γ rays. On the other hand, the 191.91-keV γ ray exhibited a delayed distribution, compared with the prompt one of the 195.3-keV γ ray as depicted in Fig. 4. The half-life of the 191.91-keV γ ray was determined to be 22(3) ns from its decay curve. The centroid of its time distribution was also shifted by 29(4) ns with respect to that of the 195.3-keV γ ray. The centroid shift of 29(4) ns corresponds to the 20(3) ns half-life, which is consistent with the result of the decay curve analysis.

The 221.5-keV γ ray observed in the prompt spectrum is attributed to the α decay of ^{253}No [13] which was possibly produced via the ^{246}Cm(^{12}C,5n) reaction. The observed γ-ray intensity is consistent with the interpretation that the ^{253}No was produced in the reaction with ^{246}Cm whose abundance is 3.1%. This γ ray was coincident with 7931–8068-keV α particles. The highest α energy of 8068 keV plus γ energy of 221.5 keV with a correction for α recoil ($8068 \times 255/251 + 221.5$) becomes 8419 keV, which is in good agreement with

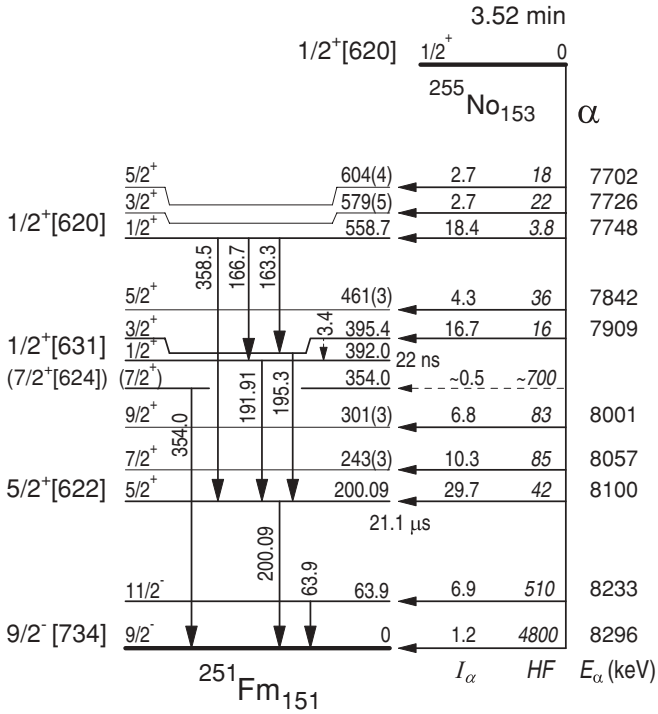

FIG. 3. Proposed decay scheme of ^{255}No. The γ-ray and level energies are given in keV. Relative intensities of α transitions (I_α) are given as the total α intensity becomes 100. The α intensity to the 354.0-keV level is calculated from the intensity of the 354.0-keV γ ray. Existence of the 3.4-keV transition between the 395.4- and 392.0-keV levels is evaluated from the intensity imbalances between the 191.91- and 166.7-keV cascade transitions and between the 195.3- and 163.3-keV ones.

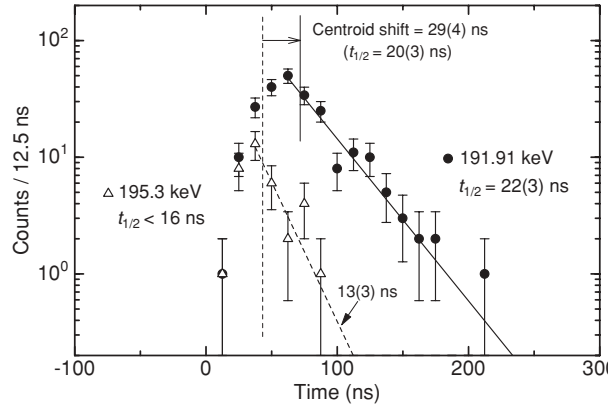

FIG. 4. Time distributions for the intervals between α and γ detections for the 191.91- and 195.3-keV γ rays. The 195.3-keV γ ray shows a prompt time distribution; the upper limit of $t_{1/2} < 16$ ns is derived from the decay curve with a 13(3) ns slope. Compared with the 195.3-keV γ ray, the decay curve of the 191.91-keV γ ray exhibits a longer half-life of 22(3) ns. The centroid of its time distribution is also shifted by 29(4) ns with respect to that of the 195.3-keV γ ray. The centroid shift of 29(4) ns corresponds to the 20(3) ns half-life, consistent with the result of the decay curve analysis.

the Q_α value of ^{253}No (8411 keV). The 221.5-keV γ ray is reported to be the most intense among those in the α decay of ^{253}No [13]. Other weak γ rays of 151 and 280 keV were not observed in our spectrum because of low statistics.

The 354.0-keV γ-ray events were weakly observed in coincidence with 7863–7970-keV α particles. The sum of the γ and α energies leads to $Q_\alpha = 8451$ keV, which is consistent with the Q_α value of ^{255}No (8428 keV) within α energy resolution. Heßberger *et al.* [11] incorporated this 354.0-keV transition between the 354.0-keV $(7/2^+)$ state and the $9/2^-$ ground state which has an $E1$ multipolarity. The present result is consistent with this assignment.

Figure 5(a) shows a decay curve of the α particles of ^{255}No. To avoid a little contamination by the 8222- and 8323-keV α particles of ^{257}No ($T_{1/2} = 24.5$ s) produced via the ^{248}Cm(^{12}C,3n) reaction, only the α counts at the range of 7510–8150 keV are used in the half-life analysis. Other possible contaminants are the 8004-keV α particles of ^{253}No (1.7 min) and the 8093-keV ones of ^{254}No (55 s) which are produced via the ^{246}Cm(^{12}C,xn)^{253,254}No and ^{248}Cm(^{12}C,6n)^{254}No reactions. The α counts of ^{253}No in the spectrum were calculated from the 221.5-keV γ-ray counts observed in the α-γ coincidence spectrum, and those of ^{254}No were estimated from the assumption that the production cross section of ^{254}No was four times larger than that of ^{253}No [14].

It was estimated that 0.9% and 3% of total α counts at the range of 7510–8150 keV should originate from the α decay of ^{253}No and ^{254}No, respectively. We subtracted these α counts from the measured ones, and fitted an exponential function to those counts as shown in Fig. 5. The deduced half-life of 3.52(21) min is a little longer than the literature value of 3.1(2) min [3] probably due to the contamination by the α decays of ^{253,254,257}No in the literature data. Note that if

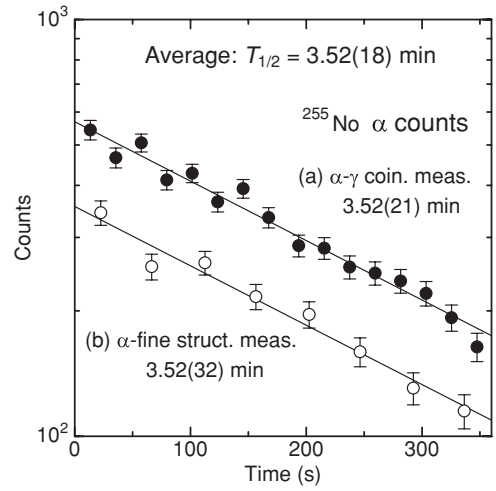

FIG. 5. Decay curves of the α particles of ^{255}No obtained (a) in the α-γ coincidence measurement and (b) in the α fine-structure measurement. To avoid a little contamination by the 8222- and 8323-keV α particles of ^{257}No, only the α counts observed in the region of 7510–8150 keV were used in the half-life analysis. The contamination by the 8004-keV α particles of ^{253}No and the 8093-keV ones of ^{254}No was estimated from the observed 221.5-keV γ-ray counts and from the production cross sections, respectively (see text), and their α counts were subtracted from the measured ones.

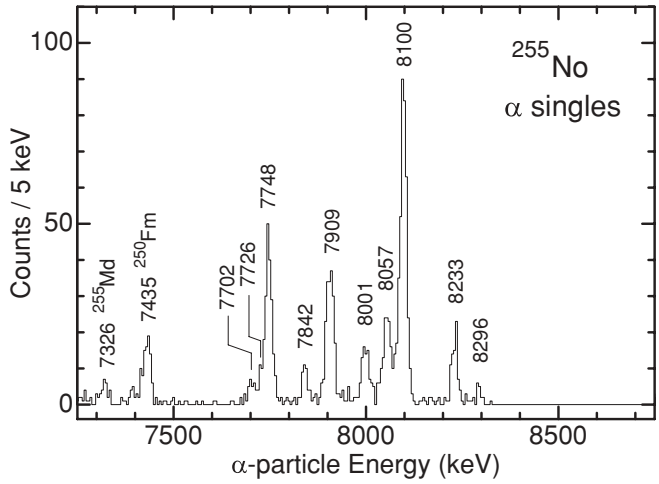

FIG. 6. α fine-structure spectrum of ^{255}No measured during the period of 90–360 s after the ends of the source depositions.

the α counts of ^{253,254}No are not subtracted in the present analysis, the half-life becomes 3.32 min. Moreover, if the 7510–8360-keV α counts are used in the analysis (which additionally include the α counts of ^{257}No), the decay curve exhibits a 3.16-min half-life.

B. α fine-structure measurement

Figure 6 shows a sum of α singles spectra measured with the detectors at the second, third, and fourth stations. Owing to the small solid angle of the detectors, the spectrum showed better energy resolution of 17 keV (full width at half maximum) and a much smaller low-energy tail of α peaks than those of the spectra measured in the α-γ experiment. (Compare Fig. 6 with Fig. 2.) This allowed us to observe weak α lines located closely at the low-energy side of the intense 7748-, 7909-, and 8100-keV α peaks. Moreover, the measurement with a small solid angle significantly reduces the influence of the coincidence summing effect, which enabled us to determine α energies and intensities very precisely, as summarized in Table II. Although the influence of the coincidence summing effect is small, the correction for that effect was carried out in determining the α energies and intensities; it was typically 10%–20% for the α intensities, and less than 1.7 keV for the α energies, which were calculated on the basis of the proposed decay scheme and the efficiency of the Si detector. α counts of ^{253,254}No included by the 8001-, 8057-, and 8100-keV α peaks were estimated by using the production ratios determined in the analysis of the α-γ experiment. The contribution of the short-lived ^{257}No is negligible because we did not use the data of the first Si detector (data of first 90 s) in the intensity analysis.

TABLE II. Energies and relative intensities of α transitions in the α decay of ^{255}No. The populated level energies in the daughter nucleus are calculated from the α-transition energies, and are compared with those determined from the γ energies.

Energy (keV)	Relative intensity[a]	Excited-state energy (keV)	
		From α energies	From γ energies
7702(5)	9.0(20)	604(4)	
7726(6)	9.1(29)	579(5)	
7748(3)	62(5)	557.3(18)	558.7(2)
7842(4)	14.4(22)	461(3)	
7909(3)	56(4)	393.8(18)	395.4(2)
8001(4)	22.8(26)	301(3)	
8057(4)	34.7(31)	243(3)	
8100(3)	100(5)	200.09[b]	200.09(11)
8233(4)	23.1(26)	64.6(28)	63.9(8)
8296(6)	4.0(12)	0.7(52)	0

[a]For I_α per 100 α decays, multiply by 0.297.
[b]Normalized at this level.

In Table II are also summarized excited-state energies calculated from the differences between α energies (corrected by a factor of 255/251) together with those from the γ-ray energies. Both the excited-state energies agree very well with each other within $\pm$1.6 keV. In this α fine-structure analysis, we established additional five excited states in ^{251}Fm which could not be observed in the γ-ray measurements.

The 7726-keV α line is not clearly seen in the spectrum. However, as discussed later, if the 7702- and 7748-keV α lines are the transitions to the $5/2^+$ and $1/2^+$ states in the $1/2^+[620]$ band, respectively, the transition to the $3/2^+$ state in the same band should also be observed at between 7702 and 7748 keV. Thus we extracted this third component from the 7702–7748-keV α group through a fitting procedure.

Figure 5(b) shows a decay curve of the α particles of ^{255}No obtained in the α fine-structure measurement. Only the α counts observed in 7510–8150 keV were used in the analysis. The contamination by the ^{253,254}No α particles were estimated in the same manner as described in the intensity analysis. By taking a weighted average of 3.52(32) min obtained in this measurement and 3.52(21) min in the α-γ experiment, the half-life of ^{255}No was determined to be 3.52(18) min.

The α-decay branch of ^{255}No was determined to be $\alpha/(\alpha + \mathrm{EC}) = 0.30(5)$ from the observed α counts of ^{255}No and its EC-decay daughter ^{255}Md. A weak α line at 7326 keV in Fig. 6 is attributed to the α decay of ^{255}Md [15]. Since the direct production of ^{255}Md via the ^{248}Cm(^{12}C,$p4n$)^{255}Md reaction is expected to be negligible, we assume here that the observed ^{255}Md mostly originated from the EC decay of ^{255}No. This assumption was confirmed by the observation of the growth of the 7326-keV α counts in the present half-life analysis. To derive the above decay branch, we adopted a literature value of 7% for the 7326-keV α-transition intensity in the decay of ^{255}Md [15]. The present α-decay branch of 0.30 for ^{255}No is about a factor of 2 smaller than the literature value of 0.614(25) [16]. In Ref. [16], ^{255}No was produced in the reaction of a ^{249}Cf target with a 73-MeV ^{12}C projectile, and the α-decay branch of ^{255}No was determined from the intensity ratio between α particles of ^{255}No and its EC-decay product ^{255}Md observed in the chemically purified nobelium fraction. However, this reaction also produces a large amount of ^{254}No whose production cross section is about a factor of 2 larger than that of ^{255}No [9]. This ^{254}No contaminates the α spectrum of ^{255}No, which could make the α-decay branch of ^{255}No overestimated. The α-decay branch is used to calculate hindrance factors of α transitions. We adopt the present α-decay branch of 0.30 in the following discussion.

IV. DISCUSSION

A. Spin-parities and configurations

It is known that the ground state of ^{251}Fm has the $9/2^-[734]$ configuration [17]. This is the start point of the following spin-parity and configuration assignments for the excited states in ^{251}Fm.

The first-excited state at 63.9 keV is considered to be the $11/2^-$ member of the $9/2^-[734]$ band. Its energy is very close to that of the $9/2^-[734]$ band in neighboring nuclei [3]. The total internal conversion coefficient of $\alpha_T = 48(31)$ is derived from the I_α value of the 8233-keV α transition and the I_γ of the 63.9-keV γ ray. Theoretical α_T values are 0.502, 42.5, and 222 for $E1$, $M1$, and $E2$ transitions, respectively [18], indicating that the 63.9-keV transition is $M1$ dominant. This also supports the $11/2^-$ assignment for the 63.9-keV level [6,8].

The 200.09-, 243-, and 301-keV levels are assigned to be the $5/2^+$, $7/2^+$, and $9/2^+$ members of the $5/2^+[622]$ band, respectively. From the K x to γ intensity ratio in the delayed coincidence spectrum [Fig. 1(b)], the K internal conversion coefficient of the 200.09-keV transition is determined to be $\alpha_K = 16.7(27)$. Theoretical α_K values of the 200.09-keV transition are 0.0878, 5.50, 0.134, 15.4, and 0.219 for $E1$, $M1$, $E2$, $M2$, and $E3$ transitions, respectively [18], indicating that the 200.09-keV transition should have an $M2$ multipolarity. The long half-life of 21.1(19) μs also supports the $M2$ assignment. The $M2$ transition to the $9/2^-$ ground state suggests that the 200.09-keV level should have a spin-parity of $5/2^+$ or $13/2^+$. Between them, the $13/2^+$ assignment is excluded, because the $13/2^+$ state should decay to the 63.9-keV $11/2^-$ state via a fast $E1$ transition. Therefore a spin-parity of $5/2^+$ is assigned to the 200.09-keV level.

As shown in Fig. 2(a), the 243- and 301-keV levels populated by the 8057- and 8001-keV α transitions do not emit any prompt γ rays, but emit intense L x rays. This indicates that the 243- and 301-keV levels decay to the 200.09-keV level via highly converted low-energy transitions. This decay pattern suggests that both the 243- and 301-keV levels should be the members of the rotational band built on the 200.09-keV $5/2^+$ state. Around $N = 151$, only the $5/2^+[622]$ neutron orbital exists near the Fermi surface with $\Omega^\pi = 5/2^+$. The energy spacings of the 200.09-, 243-, and 301-keV levels are very close to those of the $5/2^+$, $7/2^+$, and $9/2^+$ members of the $5/2^+[622]$ band in the neighboring isotones ^{247}Cm and ^{249}Cf [3].

Figures 7(a) and 7(b) show γ-ray spectra observed in coincidence with the 7909- and 7748-keV α groups, respectively. In Fig. 7(a), two γ lines at 191.91 and 195.3 keV are observed in addition to Fm K x rays. From the K x to γ intensity ratio, the upper limit of $\alpha_K < 2.0$ is deduced for the 191.91-keV transition, where the contribution of the 195.3-keV transition was estimated using theoretical α_K values for the probable multipolarities of $E1$, $M1$, and $E2$ [18]. Theoretical α_K values of the 191.91-keV transition are 0.0958, 6.19, and 0.136 for $E1$, $M1$, and $E2$, respectively [18]. The $\alpha_K < 2.0$ clearly indicates that the multipolarity of the 191.91-keV transition should be $E1$ or $E2$. As discussed later, the long half-life of 22(3) ns suggests that the 191.91-keV transition should be a hindered $E2$ transition. These results firmly assign the $E2$ multipolarity to the 191.91-keV transition. The hindered $E2$ transition to the $5/2^+$ state but no transitions to the $7/2^+$ and $9/2^+$ members of the same band indicates that the spin-parity of the 392.0-keV level should be $1/2^+$. For the 195.3-keV transition, $\alpha_K = 8.2(29)$ is derived from the measured K x to γ intensity ratio, where the contribution of the 191.91-keV $E2$ transition is calculated using the theoretical value of $\alpha_K = 0.136$. Theoretical α_K values for the 195.3-keV transition are 0.0923, 5.89, and 0.135 for $E1$, $M1$, and $E2$, respectively [18], leading to the $M1$ assignment to the 195.3-keV transition.

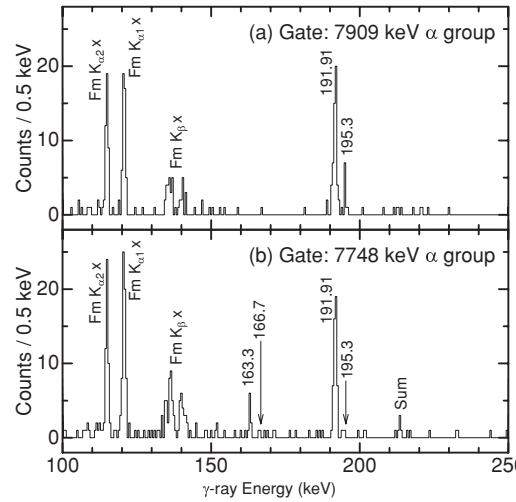

FIG. 7. Gamma-ray spectra obtained in coincidence with (a) the 7909-keV α group and (b) the 7748-keV one.

The 191.91-keV γ rays are also seen in Fig. 7(b), indicating that the 392.0-keV level is populated via γ transitions from the 558.7-keV level. If the 166.7-keV transition were only the transition linking between the 558.7-keV level and the 392.0-keV one, the intensities $I_\gamma(1 + \alpha_T)$ of the 166.7- and 191.91-keV transitions in Fig. 7(b) would be identical. However, the intensity of the 166.7-keV γ ray in Fig. 7(b) is much weaker than that of the 191.91-keV one, even if the factor of $(1 + \alpha_T)$ is taken into account. The lower limit of $\alpha_T > 41$ is obtained, while the theoretical values are 0.174, 11.9, and 2.82 for 166.7-keV $E1$, $M1$, and $E2$ transitions, respectively [18]. This indicates that another pass linking between the 558.7- and 392.0-keV levels must exist. Similar to the case of the 166.7–191.91-keV cascade, the intensities of the 163.3- and 195.3-keV transitions are not balanced in Fig. 7(b); the 195.3-keV γ ray is observed very weakly compared with the 163.3-keV one. These intensity imbalances clearly indicate the existence of the intense 3.4-keV transition between the 395.4- and 392.0-keV levels which competes with the 195.3-keV $M1$ transition. Such a low-energy transition is reported as well in ^{245}Cm [19]: the 5.5-keV transition from the $3/2^+$ to $1/2^+$ state in the $1/2^+[631]$ band. The $1/2^+[631]$ band has a large negative decoupling parameter. The energy spacing of 3.4 keV is very reasonable to assign the $1/2^+[631]$ configuration to the 395.4- and 392.0-keV levels. To reproduce the observed γ-ray intensities in Figs. 7(a), 7(b), and 1(a), the 3.4-keV transition should have an approximately 70% contribution to the total transition intensities depopulating the 395.4-keV level, and

the α branch to the 392.0-keV level should be much smaller than that to the 395.4-keV level.

In the α-γ-γ coincidence analysis, the 163.3- and 166.7-keV γ rays were observed in coincidence with the 191.91-keV γ ray. Although their statistics were only one count for each, this observation further supports the existence of the 3.4-keV transition.

The 461-keV level is considered to be the $5/2^+$ member of the $1/2^+[631]$ band. No γ ray depopulating this level was observed in the present experiment, suggesting that this level is mainly depopulated by the highly converted intraband transitions. The energy spacing between the 395.4- and 461-keV levels is 65.6(30) keV, which is consistent with that between the $3/2^+$ and $5/2^+$ members of the $1/2^+[631]$ band; in ^{247}Cm this energy is 63.1(1) keV [6]. Although the energy spacing between the $1/2^+$ and $5/2^+$ states is more suitable for such comparison, the $1/2^+$ bandhead is not reported in ^{247}Cm [6]. For ^{249}Cf, the energy of the $5/2^+$ state is not accurate [7]. As described in the next subsection, hindrance factors of α transitions also support the $1/2^+[631]$ assignment to the 461-keV level.

The intensity balance between the 163.3 + 166.7-keV and 191.91 + 195.3-keV transitions in Fig. 7(b) indicates that the 163.3-keV transition should have a large α_T value of > 5.5, leading to the $M1$ assignment to the 163.3-keV transition. The 558.7-keV level is depopulated by the γ transitions to the $1/2^+$, $3/2^+$, and $5/2^+$ states, and that to the $3/2^+$ state is an $M1$ transition. This confines the spin-parity of the 558.7-keV level to $1/2^+$, $3/2^+$, and $5/2^+$. As discussed later, the α transition to the 558.7-keV level is a favored transition with a hindrance factor of 3.8, indicating that the 558.7-keV level should be a bandhead of a one-quasiparticle state with the configuration the same as that of the ground state of ^{255}No. Neutron orbitals expected to become the ground state in the $N = 153$ isotone with $\Omega^\pi = 1/2^+$, $3/2^+$, or $5/2^+$ are the $1/2^+[620]$ and the $3/2^+[622]$ ones. Between them, the $1/2^+[620]$ configuration is more reasonable according to the consideration on their rotational-band energies. In the present experiment, the 604-keV level is clearly seen in the α fine-structure spectrum, which would be the member of the rotational band built on the 558.7-keV bandhead. Energy spacings between the $1/2^+$ and $3/2^+$ states and between the $1/2^+$ and $5/2^+$ ones in the $1/2^+[620]$ band are 29 and 45 keV in ^{247}Cm, respectively, and 23 and 43 keV in ^{249}Cf, respectively [6,7]. That between the 558.7-keV and 604-keV levels in ^{251}Fm is 45 keV, consistent with the interpretation that the 604-keV level is the $5/2^+$ member of the $1/2^+[620]$ band. On the other hand, energy spacings between the $3/2^+$ and $5/2^+$ states and between the $3/2^+$ and $7/2^+$ ones in the $3/2^+[622]$ band are 34 and 81 keV, respectively, in both ^{249}Cm and ^{251}Cf [3], and 35 keV for the $5/2^+$ state in ^{253}Fm [20]. Those spacings are not fit to the present value of 45 keV, indicating that the $3/2^+[622]$ assignment is unlikely.

The 354.0-keV level is depopulated by the single γ transition to the $9/2^-$ ground state. Although we could not obtain enough statistics to assign spin-parity and configuration to this level, this decay pattern is consistent with the $7/2^+[624]$ configuration. In ^{247}Cm and ^{249}Cf, the $7/2^+[624]$ state decays with an emission of the intense $E1$ γ ray to the $9/2^-[734]$ ground state [6,8]. On the other hand, the γ transition from the $7/2^+[613]$ state to the $9/2^-[734]$ ground state is much weaker than that to the $5/2^+[622]$ state in ^{249}Cf [8], suggesting that the $7/2^+[613]$ assignment is unlikely to the 354.0-keV level. Heßberger *et al.* [11] also suggested the $7/2^+[624]$ configuration to the 354.0-keV level owing to the deduced multipolarity of $E1$ or $E2$ for the 354.0-keV γ transition.

B. Hindrance factors of α transitions

To further confirm the $1/2^+[620]$ assignment to the ground state of ^{255}No, hindrance factors of α transitions from ^{255}No to ^{251}Fm are compared with those of lighter isotones. The ground states of the lighter $N = 153$ isotones ^{251}Cf and ^{253}Fm have the $1/2^+[620]$ configuration, and their α-transition intensities were measured very precisely [6,7]. As shown in Table III, hindrance factors of α transitions to every rotational-band

TABLE III. Hindrance factors of α transitions from the $1/2^+[620]$ ground states in the $N = 153$ isotones ^{251}Cf, ^{253}Fm, and ^{255}No to excited states in the $N = 151$ daughters. They were calculated on the basis of the Preston's spin-independent theory [21] using the radius parameters given in Refs. [22,23].

Nilsson orbital	Populated level	Hindrance factor		
		^{251}Cf $\rightarrow$ ^{247}Cm	^{253}Fm $\rightarrow$ ^{249}Cf	^{255}No $\rightarrow$ ^{251}Fm
$1/2^+[620]$	$5/2^+$	11	17	18
	$3/2^+$	19	23	22
	$1/2^+$	2.6	3.0	3.8
$1/2^+[631]$	$5/2^+$	32	31	36
	$3/2^+$	11	11	16
$5/2^+[622]$	$9/2^+$	77	48	83
	$7/2^+$	134	72	85
	$5/2^+$	31	25	42
$9/2^-[734]$	$11/2^-$	512	350	510
	$9/2^-$	5100	3200	4800

member of the $9/2^-[734]$, $5/2^+[622]$, $1/2^+[631]$, and $1/2^+[620]$ bands in the α decay of ^{251}Cf and ^{253}Fm are very similar to those observed in the α decay of ^{255}No, which strongly supports the present configuration assignments for the ground state of ^{255}No as well as for the excited states in ^{251}Fm.

The α intensity to the 354.0-keV level is calculated from the intensity of the 354.0-keV γ ray through the assumption that the 354.0-keV γ ray is only the transition depopulating the 354.0-keV level. However, the deduced hindrance factor of 700^{+500}_{-300} is about four times larger than the measured value of 170 in the α decay of ^{251}Cf to the $7/2^+[624]$ state in ^{247}Cm [6]. The $7/2^+[624]$ state in ^{247}Cm and ^{249}Cf decays not only through the intense $E1$ γ transition to the $9/2^-[734]$ ground state but also through highly converted $M1/E2$ transitions to the $5/2^+[622]$ rotational band with a comparable intensity [6,8]. The present large hindrance factor implies an existence of missing γ transitions from the $7/2^+[624]$ state to the $5/2^+[622]$ one in ^{251}Fm.

Since the α transition from $1/2^+[620]$ to $1/2^+[631]$ is a spin-flip transition, transitions with $L < K_i + K_f(=1)$ waves are strongly retarded [24], where K_i and K_f are the K quantum number of initial and final states, respectively. Thus the transition to the $1/2^+$ state in the $1/2^+[631]$ band should be hindered, while that to the $3/2^+$ state should be observed intensely, consistent with the experimental data in the α decay of ^{251}Cf and ^{255}No. For the α decay of ^{253}Fm, the 550- and ~606-keV levels populated by the 6550- and 6496-keV α transitions were evaluated to be the $(1/2^+)$ and $(5/2^+)$ states in the $1/2^+[631]$ band, respectively [3]. However, their spin-parity assignments should be revised as $3/2^+$ and $5/2^+$ according to the above consideration.

In Ref. [10], the 395.4- and 461-keV levels in ^{251}Fm (these energies were reported as 385 and 433 keV in Ref. [10]) were considered to be the members of the $7/2^+[613]$ band. This assignment is found to be incorrect owing to the present experimental results as well as the recent result in Ref. [11]. In Ref. [11], the spin-parity of $(3/2^+)$ was suggested to the tentatively assigned 395.4-keV level, and a possibility of the $3/2^+[622]$ assignment to this level was mentioned. The $1/2^+[631]$ assignment to this level was excluded because the energy spacing of 3.4 keV was considered to be too small for that between the $1/2^+$ and $3/2^+$ states in the $1/2^+[631]$ band. However, as discussed above, the energy spacing of 3.4 keV is very reasonable for the $1/2^+[631]$ band, and the hindrance factors also support the $1/2^+[631]$ configuration.

The α fine-structure data were also reported in the previous papers [9–11], but their α energies and intensities are very different from those in the present work because of the influence of the coincidence summing effect and insufficient α energy resolution. A good example is the energy of the first excited $11/2^-$ state in ^{251}Fm; this energy was reported as 50 keV [9], 46 keV [10], and $(35 + x)$ keV [11], while the present value is 63.9 keV. The intensities of the α transitions to the ground and the first-excited states in Refs. [9–11] also show large deviations from the present values owing to the coincidence summing effect.

C. Lifetimes of γ transitions

The γ transition from the $1/2^+[631]$ bandhead to the $5/2^+[622]$ one is a pure $E2$ transition with a single-particle character. The lifetimes of the $1/2^+[631] \rightarrow 5/2^+[622]$ transitions were systematically measured by Yates *et al.* [25] in various actinide nuclei, and their reduced transition probabilities $B(E2)$ were found to be 0.02–0.1 W.u. Such hindered $E2$ transitions exhibit half-lives of the order of ns–μs, which helps us distinguish $E2$ transitions from $M1$.

In Table IV, we summarize experimental $B(E2)$ values of the $1/2^+[631] \rightarrow 5/2^+[622]$ transitions. We can see the systematical trend that the $B(E2)$ value increases with the neutron number, that is, they are ~0.03 W.u. in $N = 147$ isotones, ~0.1 W.u. in $N = 149$, and 0.4 W.u. in $N = 151$. Yates *et al.* [25] pointed out that those hindrances arise from the pairing factor $P = (U_i U_f - V_i V_f)^2$, where V and U are the occupation probability of particles and holes, respectively. The relatively large $B(E2)$ value of 0.41 W.u. in ^{251}Fm implies that both the $1/2^+[631]$ and $5/2^+[622]$ orbitals would be fully occupied by neutrons in the $N = 151$ nucleus, while those in the $N = 147$ and 149 nuclei are partially occupied, which are expected from the facts that the $1/2^+[631]$ and $5/2^+[622]$ orbitals become the ground state at around $N = 145$ and 147, respectively, and that a large energy gap exists at $N = 150$ as well as at $N = 152$ in deformed neutron orbitals.

In addition to the $1/2^+[631] \rightarrow 5/2^+[622]$ transitions, the $1/2^+[620] \rightarrow 5/2^+[622]$ transitions also show long half-lives;

TABLE IV. $B(E2)$ values of $1/2^+[631] \rightarrow 5/2^+[622]$ and $1/2^+[620] \rightarrow 5/2^+[622]$ transitions in various actinide nuclei.

Nuclide	E_{level} (keV)	$t_{1/2}$	E_γ (keV)	$B(E2)$ (W.u.)
	$1/2^+[631] \rightarrow 5/2^+[622]$			
$^{239}U_{147}$	133.7	0.78(4) μs	133.7	0.0404(21)
$^{241}Pu_{147}$	161.4	0.88(5) μs	161.4	0.0218(12)
$^{243}Cm_{147}$	87.4	1.08(3) μs	87.4	0.0313(9)
$^{243}Pu_{149}$	383.6	0.33(3) μs	96.2	0.114(10)
$^{245}Cm_{149}$	355.9	0.29(2) μs	103.0	0.105(7)
$^{251}Fm_{151}$	392.0	22(3) ns	191.9	0.41(6)
	$1/2^+[620] \rightarrow 5/2^+[622]$			
$^{245}Pu_{151}$	311	0.33(2) μs	47	0.139(8)
$^{247}Cm_{151}$	404.9	100.6(6) ns	177.5	0.1338(8)

they were measured in the $N = 151$ isotones ^{245}Pu and ^{247}Cm [4,6], and their $B(E2)$ values are calculated to be 0.139 and 0.134 W.u., respectively, as shown in Table IV. It is expected that the 358.5-keV $1/2^+[620] \rightarrow 5/2^+[622]$ transition in ^{251}Fm should also have a similar $B(E2)$ value. Assuming that the $B(E2)$ value of the 358.5-keV transition is 0.134 W.u., the half-life of the 558.7-keV level is calculated to be 0.95 ns, which is consistent with the measured value of <8 ns.

D. One-quasiparticle states in $N = 151$ isotones

Figure 8(a) shows experimental level energies of one-quasiparticle states in odd-mass $N = 151$ isotones. The data

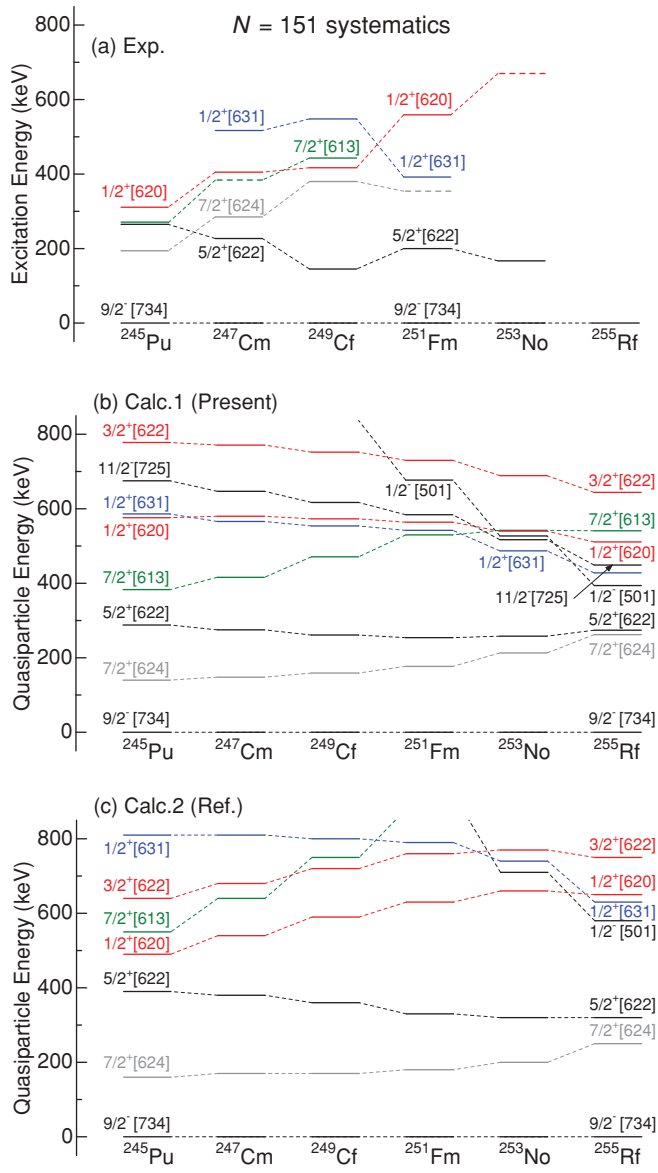

FIG. 8. (Color online) Excitation energies of neutron one-quasiparticle states in $N = 151$ isotones. (a) Experimental data. (b) Energies of one-quasiparticle states calculated in the present work. (c) Those calculated by Parkhomenko and Sobiczewski [36].

were taken from Refs. [4–8] for ^{245}Pu, ^{247}Cm, and ^{249}Cf, and from the present results for ^{251}Fm. Although several experimental data are available for excited states in ^{253}No [26–30], their configuration assignments are mostly tentative. Thus we only plotted the firmly established $5/2^+[622]$ state at 167 keV [28] and the reasonably evaluated $1/2^+[620]$ state at 670 keV [27,29] in ^{253}No. It is clearly seen that the excitation energy of the $1/2^+[620]$ state increases with the atomic number, especially at $Z \geqslant 100$. As discussed below, the $N = 152$ deformed shell gap is the gap between the $9/2^-[734]$ and $1/2^+[620]$ orbitals, or between the $9/2^-[734]$ and $7/2^+[613]$ ones at low atomic number. Thus the increase of the $1/2^+[620]$ energy indicates an increase of the $N = 152$ gap energy with increasing atomic number, especially at $Z \geqslant 100$.

The ground-state configurations of all the $N = 151$ isotones are known to be the $9/2^-[734]$. This indicates that the highest orbital located below the $N = 152$ deformed shell gap is the $9/2^-[734]$ one. The $7/2^+[624]$, $5/2^+[622]$, and $1/2^+[631]$ orbitals are known to become the ground state in $N = 149$, 147, and 145 isotones, respectively, indicating that these orbitals lie below the $9/2^-[734]$ one and these one-quasiparticle states are hole states in the $N = 151$ isotones. On the other hand, the ground-state configurations of odd-mass $N = 153$ isotones are assigned to be all $1/2^+[620]$ from $Z = 96$ (Cm) through 104 (Rf), suggesting that the lowest orbital located above the $N = 152$ deformed shell gap should be the $1/2^+[620]$ one. Other orbitals lying close to the $1/2^+[620]$ one are the $7/2^+[613]$ and $3/2^+[622]$ ones. In the $N = 153$ isotones, the $7/2^+[613]$ state is located at 49 and 106 keV higher than the $1/2^+[620]$ ground state in ^{249}Cm and ^{251}Cf, respectively, while the $3/2^+[622]$ state is at 208, 178, and 124 keV in ^{249}Cm, ^{251}Cf, and ^{253}Fm, respectively. The ground-state configurations of odd-mass $N = 155$ isotones are $1/2^+[620]$ in ^{251}Cm, $7/2^+[613]$ in ^{253}Cf and ^{255}Fm, and $3/2^+[622]$ in ^{257}No. These facts suggest that the $7/2^+[613]$ orbital lies very close to or below the $1/2^+[620]$ one at low atomic number around $Z < 96$. As the atomic number increases, the $7/2^+[613]$ orbital increases in energy relative to the $1/2^+[620]$ one, and becomes higher than the next $3/2^+[622]$ orbital around $Z > 100$. In the $N = 151$ isotones, the $7/2^+[613]$ state is located at lower energy than the $1/2^+[620]$ one in ^{245}Pu and ^{247}Cm, while in ^{249}Cf it becomes higher than the $1/2^+[620]$ one, which are consistent with the above systematics. In ^{251}Fm and ^{253}No, although there have been no experimental data for the $7/2^+[613]$ state, the $7/2^+[613]$ state is expected to lie at higher energy than the $1/2^+[620]$ one according to the above systematics.

To discuss the trends of the experimental level energies, we calculate the ground-state deformations and energies of one-quasiparticle states in the $N = 151$ isotones using the macroscopic-microscopic model whose details are described in Ref. [31]. The macroscopic part of the model is calculated with the finite-range liquid-drop model (FRLDM) [31]. The parameters correspond to FRLDM(2002) [32]. For the microscopic part, we use the folded-Yukawa single-particle potential. The pairing effect is calculated with the Lipkin-Nogami model [33–35]. The ground-state deformation is calculated by minimizing the total energy of the nucleus in

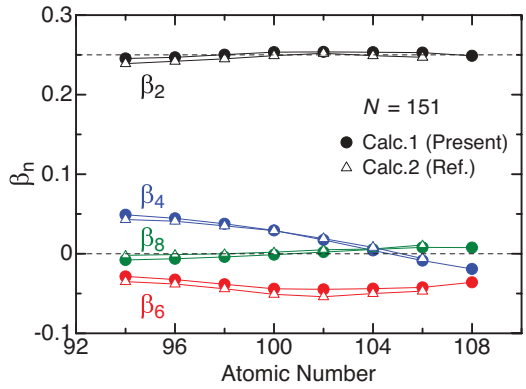

FIG. 9. (Color online) Deformation parameters $\beta_{2,4,6,8}$ for $N = 151$ isotones calculated in the present work and those in Ref. [36].

a four-dimensional deformation space with the deformation parameters $\beta_{2,4,6,8}$. The deformation parameters obtained in the present work are given in Fig. 9. The one-quasiparticle energy E_κ is calculated by the equation defined in the Lipkin-Nogami model:

$$E_\kappa = \sqrt{(\epsilon_\kappa - \lambda)^2 + \Delta^2} + \lambda_2, \qquad (1)$$

where ϵ_κ is the shifted single-particle energy for a given orbital κ, λ is the Fermi energy, Δ is the pairing gap, and λ_2 is the number-fluctuation constant. The energies of the calculated neutron one-quasiparticle states are given in Fig. 8(b). The deformation parameters and the energies of one-quasiparticle states in another macroscopic-microscopic calculation by Parkhomenko and Sobiczewski [36] are also shown for comparison in Figs. 9 and 8(c), respectively. They used a Woods-Saxon single-particle potential for describing single-particle properties of a nucleus and the BCS approximation for the pairing effect. It is found that the deformation parameters obtained in both the calculations are nearly identical.

As shown in Figs. 8(b) and 8(c), the ground-state configurations of all the $N = 151$ isotones are calculated to be the $9/2^-[734]$. This orbital lies just below the $N = 152$ deformed shell gap. The orbital lying just above the $N = 152$ gap is the $1/2^+[620]$ or the $7/2^+[613]$ one. In the present calculation, the $7/2^+[613]$ state is located at lower energy than the $1/2^+[620]$ one in ^{245}Pu, ^{247}Cm, ^{249}Cf, and ^{251}Fm, indicating that the $N = 152$ deformed shell gap is the gap between the $9/2^-[734]$ and $7/2^+[613]$ orbitals. The energies of the calculated $7/2^+[613]$ states in the isotones show a gradual increase with the atomic number. This indicates that the present calculation reasonably reproduces the experimental trend that the $N = 152$ gap energy increases with the atomic number, although the lowest orbital above the $N = 152$ gap is not the $1/2^+[620]$ one but the $7/2^+[613]$ one in this calculation. On the other hand, the $1/2^+[620]$ states exhibit nearly constant excitation energy in the calculation. This atomic-number dependence is much weaker than the experimental one.

In the calculation by Parkhomenko and Sobiczewski [36], the $1/2^+[620]$ state is located at lower energy than the $7/2^+[613]$ one in all the isotones, indicating that the $N = 152$ deformed shell gap is the gap between the $9/2^-[734]$ and $1/2^+[620]$ orbitals. Their calculation shows a gradual increase of the $1/2^+[620]$ energy with increasing atomic number, but its Z dependence is smaller than the experimental one at $Z \geqslant 100$. Qian *et al.* [29] also calculated the energies of the $1/2^+[620]$ states in the $N = 151$ isotones using the deformation parameters taken from Ref. [31] and with a Woods-Saxon potential. They reproduced well the energies of the $1/2^+[620]$ states as well as their gradual increase from

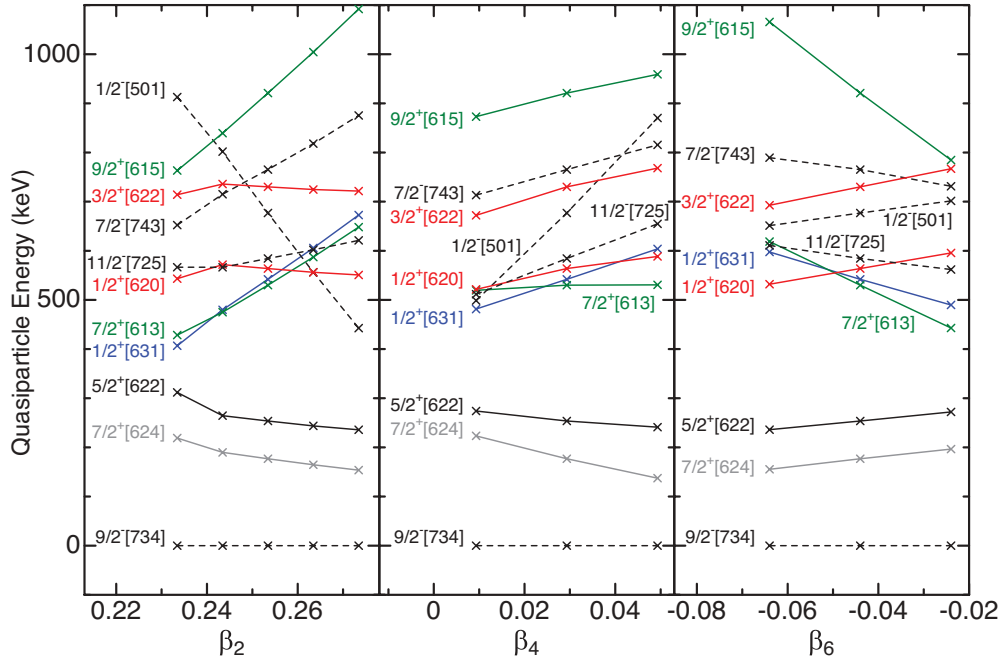

FIG. 10. (Color online) Energies of neutron one-quasiparticle states in ^{251}Fm calculated as a function of deformation parameters $\beta_{2,4,6}$.

^{245}Pu to ^{249}Cf, but could not reproduce the sizable increase of the $1/2^+[620]$ energy at $Z \geqslant 100$ as well.

In order to attempt reproducing the experimental trend of the $1/2^+[620]$ energy at $Z \geqslant 100$, we calculate the influences of the deformation parameters $\beta_{2,4,6}$ on the one-quasiparticle energies in ^{251}Fm, because single-particle energies are very sensitive to the deformation parameters. The results are shown in Fig. 10. It is clearly seen that the $1/2^+[620]$ energy is not sensitive to the $\beta_{2,4,6}$ values. This indicates that the sizable increase of the $1/2^+[620]$ energy at $Z \geqslant 100$ cannot be reproduced only by changing the deformation parameters used in the calculation.

On the other hand, energies of the $7/2^+[613]$ and $1/2^+[631]$ states are very sensitive to the deformation parameters. In general, different responses of single-particle energies to the deformation parameters reflect different density distributions of each single-particle wave function. For example, if the density distribution of a single-particle wave function overlaps well with the macroscopic nuclear shape, this single-particle orbital becomes attractive and its energy becomes low. Thus the strong β_2 and β_6 dependences of the $7/2^+[613]$ one-quasiparticle energy relative to the $9/2^-[734]$ one indicate that the density distribution of the $7/2^+[613]$ orbital differs greatly from that of the $9/2^-[734]$ one in the components of β_2 and β_6, whereas the similar β_4 components result in the weak β_4 dependence between these orbitals.

The calculated $7/2^+[613]$ energy in Fig. 8(b) increases with the atomic number up to $Z = 102$. This would result from the small increase of β_2 and the decrease of β_6 up to $Z = 102$, as shown in Fig. 9. The β_4 value does not influence the $7/2^+[613]$ energy. The small increase of β_2 and the decrease of β_6 also raise the $1/2^+[631]$ energy, while the rapidly decreasing β_4 value lowers the calculated $1/2^+[631]$ energy with increasing atomic number. The experimental $1/2^+[631]$ energy drops by about 150 keV from ^{249}Cf to ^{251}Fm. This trend is consistent with the rapidly decreasing β_4 value with increasing atomic number. A significant lowering of the $1/2^+[631]$ state with increasing atomic number is also suggested in the $N = 149$ isotones [13]. Experimental assignments of the $1/2^+[631]$ states at $Z \geqslant 102$ as well as the $7/2^+[613]$ states at $Z \geqslant 100$ in the $N = 151$ isotones will become a key to understand the evolution of nuclear deformation around the $N \approx 152$ nuclei.

V. SUMMARY

Excited states in ^{251}Fm populated via the α decay of ^{255}No have been studied in detail through α-γ coincidence and α fine-structure measurements. Five excited states reported previously [11] were firmly established through the α-γ coincidence measurement, and rotational bands built on one-quasiparticle states were newly established through the α fine-structure measurement. The α fine-structure measurement enabled us not only to observe the weak α transitions to the rotational-band members but also to determine the α energies and intensities precisely without an influence of the coincidence summing effect. The deduced hindrance factors of the α transitions and the rotational-band energies built on the one-quasiparticle states were very helpful to assign the neutron configurations to the excited states. The α-γ delayed coincidence analysis revealed that the 191.91-keV γ transition is a hindered $E2$ transition with a half-life of 22 ± 3 ns. On the basis of the deduced internal conversion coefficients, lifetimes of γ transitions, rotational-band energies built on one-quasiparticle states, and hindrance factors of α transitions, spin-parities, and neutron configurations of the excited states in ^{251}Fm as well as the ground state of ^{255}No were definitely identified without the $1/2^+[620]$ assumption for the ground state of ^{255}No.

The $N = 152$ deformed shell gap is the gap between the $9/2^-[734]$ and $1/2^+[620]$ orbitals, or between the $9/2^-[734]$ and $7/2^+[613]$ ones at low atomic number around $Z < 96$. Since all the $N = 151$ isotones have the $9/2^-[734]$ ground state, excitation energy of the $1/2^+[620]$ state in the $N = 151$ isotones reflects the $N = 152$ gap energy. It was found that the excitation energy of the $1/2^+[620]$ state in the $N = 151$ isotones increases with the atomic number, especially at $Z \geqslant 100$, indicating that the $N = 152$ gap energy increases with the atomic number.

To discuss the trends of the experimental level energies, we calculated the ground-state deformations and energies of one-quasiparticle states in the $N = 151$ isotones using the macroscopic-microscopic model which is based on the finite-range liquid-drop model and the Strutinsky shell correction method. This calculation reasonably reproduced the increase of the $N = 152$ gap energy with the atomic number, although the calculated $1/2^+[620]$ energies in the isotones showed a much weaker atomic-number dependence than the experimental one.

We also calculated the influences of the deformation parameters $\beta_{2,4,6}$ on the one-quasiparticle energies in ^{251}Fm, and found that the $1/2^+[620]$ energy is not sensitive to the $\beta_{2,4,6}$ values. This means that the $1/2^+[620]$ energy cannot be reproduced only by changing the deformation parameters used in the calculation. Further studies are needed to understand the increase of the $1/2^+[620]$ energy at $Z \geqslant 100$. On the other hand, energies of the $7/2^+[613]$ and $1/2^+[631]$ states are very sensitive to the deformation parameters. The experimental $1/2^+[631]$ energy drops by about 150 keV from ^{249}Cf to ^{251}Fm, suggesting the influence of the rapidly decreasing β_4 value with increasing atomic number. Experimental assignments of the $1/2^+[631]$ states at $Z \geqslant 102$ as well as the $7/2^+[613]$ states at $Z \geqslant 100$ in the $N = 151$ isotones will become a key to understand the evolution of nuclear deformation around the $N \approx 152$ nuclei.

ACKNOWLEDGMENTS

This work was supported in part by a Grant-in-Aid for Scientific Research of Ministry of Education, Culture, Sports, Science and Technology of Japan. T.I. thanks P. Möller for valuable discussions. The work of T.I. was done in the Yukawa International Project for Quark-Hadron Sciences (YIPQS). The numerical calculations were carried out on Altix3700 BX2 at YITP in Kyoto University.

[1] G. Audi, A. H. Wapstra, and C. Thibault, Nucl. Phys. A **729**, 337 (2003).
[2] A. Sobiczewski and K. Pomorski, Prog. Part. Nucl. Phys. **58**, 292 (2007).
[3] *Table of Isotopes*, 8th ed., edited by R. B. Firestone and V. S. Shirley (John Wiley & Sons, New York, 1996).
[4] H. Makii *et al.*, Phys. Rev. C **76**, 061301(R) (2007).
[5] T. H. Braid, R. R. Chasman, J. R. Erskine, and A. M. Friedman, Phys. Rev. C **4**, 247 (1971).
[6] I. Ahmad, R. R. Chasman, J. P. Greene, F. G. Kondev, E. F. Moore, E. Browne, C. E. Porter, and L. K. Felker, Phys. Rev. C **68**, 044306 (2003).
[7] I. Ahmad, A. M. Friedman, R. F. Barnes, R. K. Sjoblom, J. Milsted, and P. R. Fields, Phys. Rev. **164**, 1537 (1967).
[8] I. Ahmad, R. K. Sjoblom, and P. R. Fields, Phys. Rev. C **14**, 218 (1976).
[9] P. Eskola, K. Eskola, M. Nurmia, and A. Ghiorso, Phys. Rev. C **2**, 1058 (1970).
[10] P. F. Dittner, C. E. Bemis Jr., D. C. Hensley, R. J. Silva, and C. D. Goodman, Phys. Rev. Lett. **26**, 1037 (1971); C. E. Bemis Jr., D. C. Hensley, P. F. Dittner, C. D. Goodman, and R. J. Silva, Oak Ridge National Laboratory Report No. ORNL-4706, 62 (1971).
[11] F. P. Heßberger *et al.*, Eur. Phys. J. A **29**, 165 (2006).
[12] Y. Nagame *et al.*, J. Nucl. Radiochem. Sci. **3**, 85 (2002).
[13] F. P. Heßberger, S. Hofmann, D. Ackermann, P. Cagarda, R.-D. Herzberg, I. Kojouharov, P. Kuusiniemi, M. Leino, and R. Mann, Eur. Phys. J. A **22**, 417 (2004).
[14] T. Sikkeland, A. Ghiorso, and M. J. Nurmia, Phys. Rev. **172**, 1232 (1968).
[15] P. R. Fields, I. Ahmad, R. F. Barnes, R. K. Sjoblom, and E. P. Horwitz, Nucl. Phys. A **154**, 407 (1970); I. Ahmad, R. R. Chasman, and P. R. Fields, Phys. Rev. C **61**, 044301 (2000).
[16] R. J. Silva, C. E. Bemis Jr., P. F. Dittner, and D. C. Hensley, Oak Ridge National Laboratory Report No. ORNL-5137, 70 (1976).
[17] I. Ahmad, J. Milsted, R. K. Sjoblom, J. Lerner, and P. R. Fields, Phys. Rev. C **8**, 737 (1973).
[18] F. Rösel, H. M. Fries, K. Alder, and H. C. Pauli, At. Data Nucl. Data Tables **21**, 91 (1978).
[19] I. Ahmad, D. D. Sharma, and R. K. Sjoblom, Nucl. Phys. A **258**, 221 (1976).
[20] M. Asai *et al.*, Phys. Rev. Lett. **95**, 102502 (2005).
[21] M. A. Preston, Phys. Rev. **71**, 865 (1947).
[22] Y. A. Akovali, Nucl. Data Sheets **102**, 515 (2004).
[23] A. Artna-Cohen, Nucl. Data Sheets **88**, 155 (1999).
[24] J. O. Rasmussen, in *Alpha-, Beta- and Gamma-ray Spectroscopy*, edited by K. Siegbahn (North-Holland, Amsterdam, 1966), p. 701.
[25] S. W. Yates, I. Ahmad, A. M. Friedman, F. J. Lynch, and R. E. Holland, Phys. Rev. C **11**, 599 (1975).
[26] C. E. Bemis Jr., J. R. Tarrant, R. J. Silva, L. D. Hunt, D. C. Hensley, P. F. Dittner, O. L. Keller Jr., R. L. Hahn, and C. D. Goodman, Oak Ridge National Laboratory Report No. ORNL-4976, 37 (1974).
[27] F. P. Heßberger *et al.*, Z. Phys. A **359**, 415 (1997); F. P. Heßberger *et al.*, in *Experimental Nuclear Physics in Europe: Facing the Next Millennium*, edited by B. Rubio, M. Lozano, and W. Gelletly, AIP Conf. Proc. No. 495, 145 (1999).
[28] A. Lopez-Martens *et al.*, Eur. Phys. J. A **32**, 245 (2007).
[29] J. Qian *et al.*, Phys. Rev. C **79**, 064319 (2009).
[30] B. Streicher *et al.*, Eur. Phys. J. A **45**, 275 (2010).
[31] P. Möller, J. R. Nix, W. D. Myers, and W. J. Swiatecki, At. Data Nucl. Data Tables **59**, 185 (1995).
[32] P. Möller, A. J. Sierk, and A. Iwamoto, Phys. Rev. Lett. **92**, 072501 (2004).
[33] H. J. Lipkin, Ann. Phys. (NY) **9**, 272 (1960).
[34] Y. Nogami, Phys. Rev. **134**, B313 (1964).
[35] H. C. Pradhan, Y. Nogami, and J. Law, Nucl. Phys. A **201**, 357 (1973).
[36] A. Parkhomenko and A. Sobiczewski, Acta Phys. Pol. B **36**, 3115 (2005).